

LA-4518

4.3

CIC-14 REPORT COLLECTION  
REPRODUCTION  
COPY

LOS ALAMOS SCIENTIFIC LABORATORY  
of the  
University of California  
LOS ALAMOS • NEW MEXICO

Sonic Limitations and  
Startup Problems of Heat Pipes

LOS ALAMOS NATIONAL LABORATORY



3 9338 00387 2958

UNITED STATES  
ATOMIC ENERGY COMMISSION  
CONTRACT W-7405-ENG 36

## LEGAL NOTICE

This report was prepared as an account of work sponsored by the United States Government. Neither the United States nor the United States Atomic Energy Commission, nor any of their employees, nor any of their contractors, subcontractors, or their employees, makes any warranty, express or implied, or assumes any legal liability or responsibility for the accuracy, completeness or usefulness of any information, apparatus, product or process disclosed, or represents that its use would not infringe privately owned rights.

This report expresses the opinions of the author or authors and does not necessarily reflect the opinions or views of the Los Alamos Scientific Laboratory.

Printed in the United States of America. Available from  
National Technical Information Service  
U. S. Department of Commerce  
Springfield, Virginia 22151

Price: Printed Copy \$3.00; Microfiche \$0.65

Written: September 1970  
Distributed: November 1970

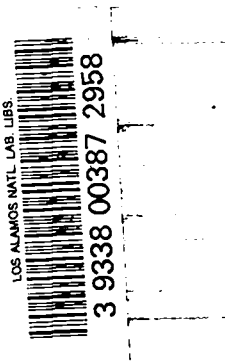
LA-4518  
UC-37, INSTRUMENTS  
TID-4500

**LOS ALAMOS SCIENTIFIC LABORATORY**  
of the  
**University of California**  
LOS ALAMOS • NEW MEXICO

**Sonic Limitations and  
Startup Problems of Heat Pipes**

by

J. E. Deverall  
J. E. Kemme  
L. W. Florschuetz\*



\* Visiting Staff Member

Present address: Department of Engineering Sciences  
Arizona State University, Tempe, Arizona.



# SONIC LIMITATIONS AND STARTUP PROBLEMS OF HEAT PIPES

by

J. E. Deverall, J. E. Kemme, and L. W. Florschuetz

## ABSTRACT

In the design of heat pipes, consideration must be given not only to the internal structure and fluid dynamics of the pipe but also to the external conditions imposed upon it. Several tests of heat pipes were made under different operating conditions to demonstrate the effect of sonic vapor velocities and related startup problems which influence heat-pipe design. Derivations are presented for the pressure, temperature, and density relationships encountered in the vapor flow stream, and tables of sonic limits for various heat-pipe fluids are included.

## INTRODUCTION

The heat pipe is a thermal conductance device which is capable of high heat-transfer rates with essentially isothermal operation;<sup>1</sup> however, it will not perform properly under all conditions. The operating characteristics of a pipe with a given geometry may vary from phenomenal to nonfunctional, and axial temperature drops of several hundred degrees may occur along the length of the pipe in some cases. The performance of a heat pipe depends not only upon the type of wick and working fluid used, but also to a high degree upon the external conditions imposed upon it.

The heat pipe is frequently considered as a simple heat-transfer structure. This concept visualizes the heat pipe as a device which:

1. Is simple to construct and operate.
2. Utilizes latent heat, providing high heat-transfer rates with very little mass flow.
3. Transfers heat isothermally.

For thermal control and some special applications, this simple concept is adequate, but

optimization of heat-pipe performance reveals that the dynamics of fluid flow are very complicated. Under certain operational conditions:

1. Vapor flow may be molecular or continuum -- compressible or incompressible.
2. Vapor velocities may be sonic or even supersonic.
3. Countercurrent flow of vapor and liquid, with communication between flow paths, may result in interaction between the vapor and the liquid.

In the design of heat pipes for high heat-transfer rates, consideration must be given to these factors, not only at design conditions, but particularly during startup.

A series of tests were made which demonstrate the effects of sonic vapor velocities upon the operational and startup characteristics of heat pipes. Appendices A and B are included to give a better understanding of the internal fluid-flow dynamics for making appropriate design adjustments to accommodate for external conditions.

### SONIC VAPOR VELOCITY

In a cylindrical heat pipe, the vapor stream accelerates and decelerates because of the change in mass flow along the pipe. Mass addition in the evaporator and mass removal in the condenser cause variations in the vapor stream velocity similar to those of the flow in a converging-diverging nozzle. Velocity variations in a converging-diverging nozzle result from a constant mass flow through a variable area, whereas in a heat pipe, velocity variations result from a variable mass flow through a constant area. The pressure decreases in the converging section of the nozzle, with a resulting increase in velocity (see Fig. 1). In the diverging section, the velocity can increase further and become supersonic, or a recompression of the gas may occur, resulting in a pressure recovery and a reduction of velocity. The amount of pressure recovery depends upon the magnitude of back pressure. Curve A shows a subsonic flow with a back pressure,  $P_a$ . The pressure decreases in the convergent section with an increase in velocity up to the throat. In the divergent section, a pressure recovery occurs with a decrease in velocity. If the back pressure is lowered to  $P_b$ , the velocity becomes sonic at the throat and the maximum mass flow rate is attained. This is considered the critical, or choked, flow condition, and further reduction of the back pressure will not increase the flow rate. When the pressure is reduced to  $P_c$ , the velocity in the divergent section becomes supersonic and pressure recovery is often in the form of a shock front. There is one value of back pressure,  $P_d$ , for a given area ratio which results in a continuous acceleration of the gas over the length of the divergent section; decreasing the back pressure below this value has no effect upon conditions in the nozzle section.

The vapor flow in a cylindrical heat pipe is quite similar to the flow characteristics encountered in a converging-diverging nozzle. Very high velocities, choked flow,

and pressure recovery are evident in heat-pipe operation and are a function of heat input and rejection rates. These flow characteristics in heat pipes have been demonstrated experimentally by Kemme<sup>2</sup> with a sodium heat pipe. The results of this test are shown in Fig. 2 with a plot of temperature vs heat-pipe length. Heat-pipe wall temperatures were plotted rather than pressure because, in heat-pipe operation, temperature is the main parameter of concern and, because a two-phase system exists, the temperature and pressure profiles are identical. A constant heat input of 6.4 kW was supplied to the evaporator section, and heat rejection was controlled by varying the helium-argon mixture in the gap of a water-cooled calorimeter. Curve A demonstrates a subsonic flow condition with a slight temperature recovery in the condenser. The temperature dropped along the evaporator section as the vapor stream was accelerated due to mass addition by evaporation. When the condenser temperature was lowered (Curve B) by increasing the heat-rejection rate, the evaporator temperatures were also lowered, the vapor velocity at the exit became sonic, and critical or choked-flow conditions existed. Increasing the heat-rejection rate further only lowered the condenser temperature because the heat-transfer rate to that section could not be increased due to the existence of choked flow. The change in condenser temperature had no effect upon the evaporator temperatures because the vapor was moving at the speed of sound at the evaporator exit and changes in condenser conditions could not be transmitted upstream to the evaporator section. This demonstrates the sonic limit of a heat pipe. At this limit there is a maximum axial heat-transfer rate due to choked flow and a fixed axial temperature drop along the evaporator associated with any given evaporator entrance temperature.

Although the flow dynamics of the heat pipe are quite similar to those of the converging-diverging nozzle, the expressions

for predicting the quantitative pressure, temperature, and density changes in the flow stream are somewhat different. The derivation of the expressions for heat pipes should be based upon flow with constant cross-sectional area and mass addition. A one-dimensional flow analysis based upon these assumptions (see Appendix A) gives the following relationships for pressure, temperature, and density changes of the vapor in the evaporator section:

$$\frac{P_o}{P_1} = 1 + kM^2, \quad (1)$$

$$\frac{T_o}{T_1} = 1 + \left(\frac{k+1}{2}\right)M^2, \quad (2)$$

$$\frac{\rho_o}{\rho_1} = \frac{1 + kM^2}{1 + \left(\frac{k+1}{2}\right)M^2}, \quad (3)$$

where

$P_o$  = static pressure at evaporator entrance,

$P_1$  = static pressure at evaporator exit,

$T_o$  = stagnation temperature of vapor at evaporator entrance,

$T_1$  = average temperature of vapor stream at evaporator exit,

$\rho_o$  = vapor density at evaporator entrance,

$\rho_1$  = vapor density at evaporator exit,

$k$  = ratio of specific heats,

$M$  = Mach number of vapor flow.

For monatomic fluids at sonic velocity ( $M = 1$ ;  $k = 1.667$ )

$$\frac{P_o}{P_1} = 2.667,$$

$$\frac{T_o}{T_1} = 1.333,$$

$$\frac{\rho_o}{\rho_1} = 2,$$

At high vapor velocities there is a large radial temperature variation across the vapor stream so the average vapor temperature,  $T_1$ , does not indicate the temperature of the vapor at the wall,  $T_{w1}$ . However, the static pressure of the vapor is

essentially constant across the stream so that  $T_{w1}$  at the evaporator exit can be estimated by using Eq. (1) to calculate the static pressure at this point. Useful graphs to determine this pressure at the evaporator exit for sonic and subsonic velocities are shown in Figs. A5 and A6, Appendix A. With the aid of appropriate saturated-vapor tables, the vapor temperature corresponding to this pressure can be determined. This estimated temperature is a close approximation of the wall temperature at the evaporator exit and is readily measured in experimental tests. The major difficulty is determining the exact location of the exit.

The maximum heat-transfer rate at sonic flow can be calculated by Levy's equation:<sup>3</sup>

$$\frac{Q_c}{A} = \frac{\rho_o V_s L}{\sqrt{2(k+1)}}, \quad (4)$$

where

$\frac{Q_c}{A}$  = maximum axial heat transfer per unit cross-sectional area with choked flow,

$\rho_o$  = vapor density at evaporator entrance,

$V_s$  = sonic velocity based upon stagnation temperature,  $T_o$ ,

$L$  = heat of vaporization,

$k$  = ratio of specific heats.

Tables of the sonic limits for various heat-pipe fluids are listed in Appendix B.

Increasing the heat-rejection rate beyond the sonic limit lowers the condenser temperature, induces supersonic vapor flow, and creates very large axial temperature gradients along the pipe but does not increase the heat-transfer rate. Consequently, when a heat pipe is operating with low vapor densities and high vapor velocities, isothermal operation is not possible.

In another experiment, Kemme<sup>2</sup> also demonstrated the behavior of this sodium pipe during startup. The axial temperature differences along the evaporator section were in close agreement with calculated

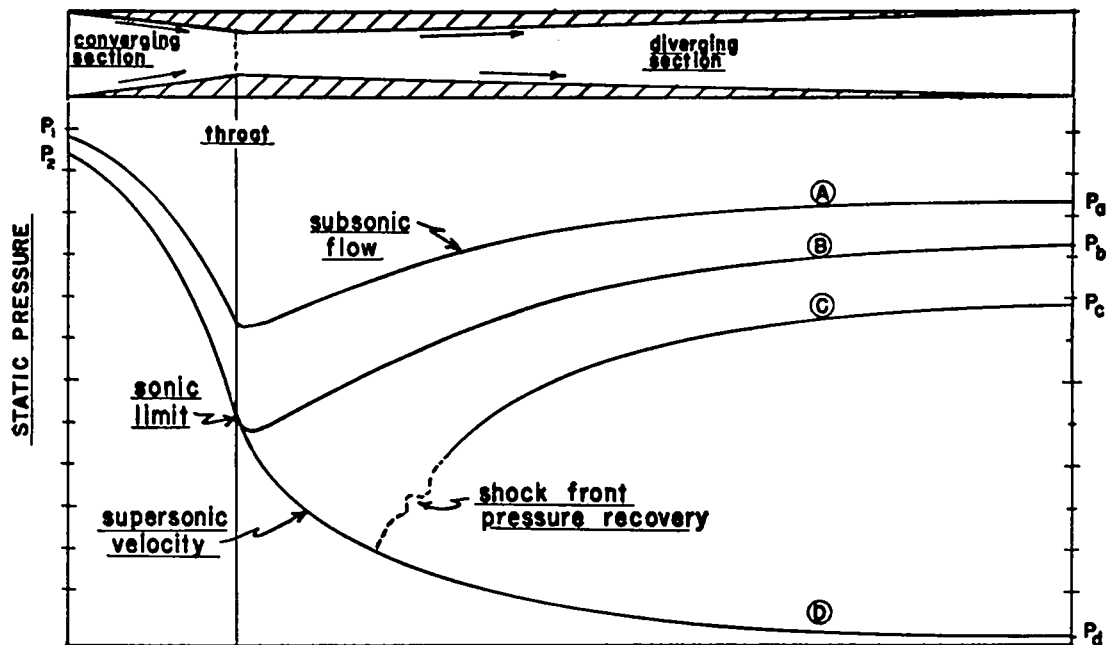


Fig. 1. Pressure profiles in a converging-diverging nozzle.

values for sonic flow. When sufficient continuum flow reached the condenser end of the pipe to start raising its temperature, the evaporator entrance temperature gradually moved away from the sonic curve, indicating a decrease in vapor velocity and an increase in vapor density. Eventually the temperature drop along the evaporator approached zero, and isothermal operation was achieved.

This indicates that a startup with sonic vapor flow is possible with carefully controlled heat input and rejection rates. However, there are some heat-pipe applications where the pipe might have to start up with full design heat input and a closely coupled heat sink, which could make startup difficult or, in some cases, impossible.<sup>4</sup>

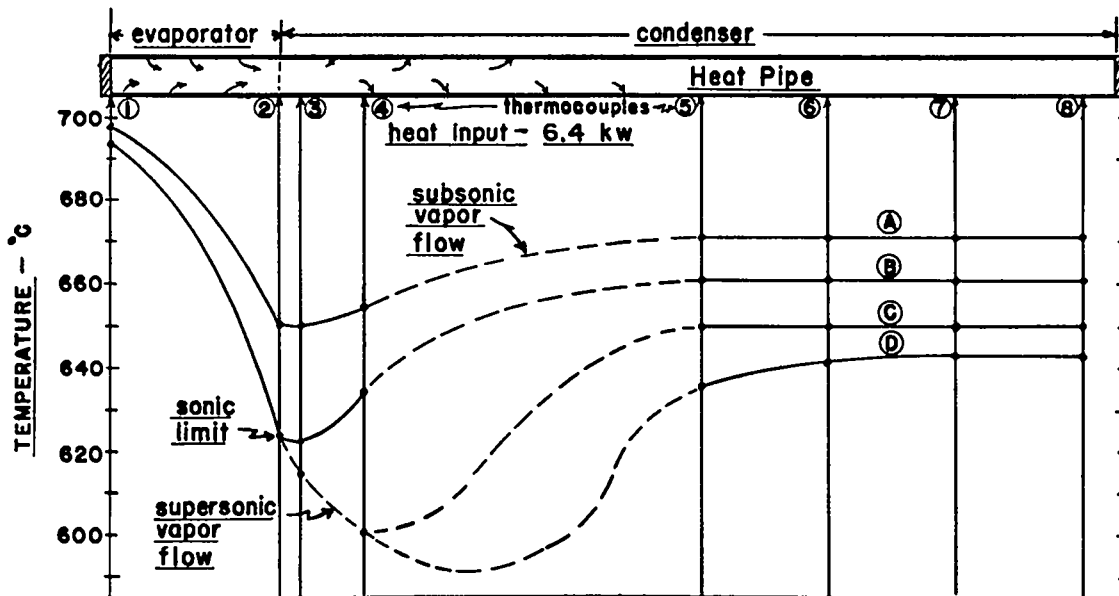


Fig. 2. Temperature profiles in a heat pipe.

## STARTUP TESTS WITH A MERCURY HEAT PIPE

### Heat-Pipe Construction

To study the startup problems encountered with heat pipes, several tests were made under different conditions with a mercury heat pipe. The heat pipe was a .600-in.-o.d. tube, 19-5/8 in. long, and contained a wick structure consisting of three layers of 100-mesh screen. Closure of the pipe was made by welding end caps into each end; one of the caps was equipped with a 1/4-in.-o.d. tube which was connected to a bellows valve for loading and sealing the pipe. All parts of the pipe were made of stainless steel and had been outgassed at 1000°C before assembly.

Heat to the pipe was supplied by a helical Nichrome wire, enclosed in insulator beads and wound around the evaporator over a length of 7 in. The winding was surrounded by a 2-in.-o.d. tube filled with insulation and sealed at the ends with alundum cement. Three thermocouples were attached to the heater winding to monitor heater temperature, and seven thermocouples were spot-welded along the length of the pipe, as shown in Fig. 3, to indicate heat-pipe temperatures. Heat was rejected to a water-cooled, gas-gap calorimeter fitted

with a  $\Delta T$  meter across the inlet and outlet connections to provide heat-balance measurements. The gas gap was fitted with a fine capillary tube so that helium could be fed into the gap to replace the air, which increased the thermal conductivity and heat-rejection rate. The pipe was loaded with mercury as the working fluid plus magnesium and titanium additions to promote wetting,<sup>5</sup> was evacuated, and sealed by closing the bellows valve. After wetting-in at 500°C for two days, the pipe was fitted with the heater, thermocouples, and calorimeter.

### Test Procedure

Tests were made under four different conditions to demonstrate the factors affecting startup:

- Test 1 - Helium in calorimeter gap.  
Pipe evacuated.
- Test 2 - Air in calorimeter gap.  
Pipe evacuated.
- Test 3 - Helium in calorimeter gap.  
Noncondensable gas in pipe.
- Test 4 - Pipe evacuated.  
Calorimeter removed.  
Heat rejection by natural convection.  
Constant heat input, 300W.

For Tests 1 through 3, the pipe was gradually heated to various temperature levels

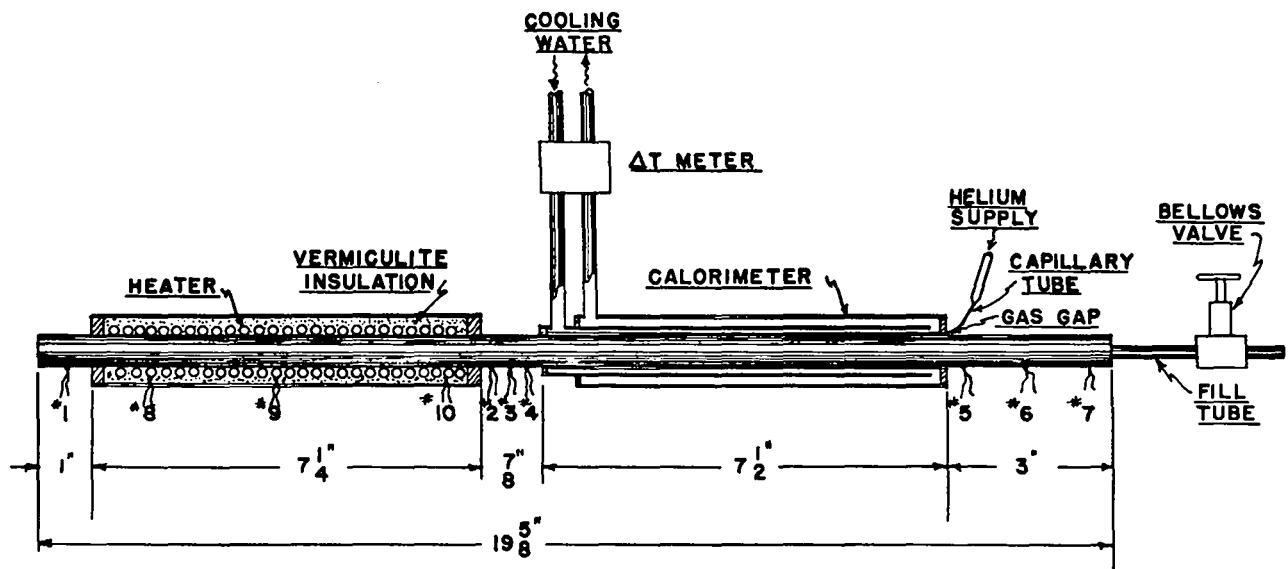


Fig. 3. Heat-pipe assembly for startup tests.

until the maximum temperature was reached. At each level, temperature equilibrium was established before taking readings and proceeding to the next level. For Test 4, the calorimeter was removed so that a low heat rejection rate could be obtained with only natural convection. More thermocouples were used, and the thermocouple spacing was rearranged to provide a more accurate picture of the temperature profiles, particularly at the condenser end of the pipe. With the pipe at room temperature, a constant power input of 300 W was applied to the evaporator and temperature gradients recorded at various time intervals.

## Results

### Test 1

This test demonstrated the failure of a heat pipe to start up because of a high heat-rejection rate with a closely coupled heat sink. As shown in Fig. 4, it was not possible to raise the temperature of the condenser section of the pipe by increasing the power input. The high heat-removal rate resulted in low vapor densities, sonic

vapor velocities, and molecular flow toward the end of the condenser. This is the sonic limit of a heat pipe which results in choked vapor flow and limited heat transfer to the condenser section. When the heat input was increased to 250 W, interaction between the liquid and vapor at these high vapor velocities eventually swept liquid out of the wick structure, causing the evaporator to dry out and overheat as indicated by Thermocouple 1. This condition is the entrainment limit and causes heat-pipe failure. Entrainment is a function of the ratio of inertial vapor forces and liquid surface tension forces

$$\frac{\rho_v V \lambda}{2 \delta}$$

where

$\rho_v$  = vapor density,

$V$  = vapor velocity,

$\lambda$  = a characteristic length dependent upon the wick structure

$\delta$  = liquid surface tension.

When this ratio exceeds unity, the inertial forces predominate and liquid droplets are swept out of the wick structure. It is often possible to hear droplets impinge on the condenser end when this limit occurs. Although the pipe could operate properly at design conditions, entrainment would cause failure during startup, and operating design conditions could not be achieved with a closely coupled high-heat-removal system. The possibility of entrainment failure can be reduced by altering the design of the wick structure to reduce  $\lambda$ .<sup>6</sup> As shown in Appendix B, a mercury heat pipe has a sonic heat-transfer rate of 20.8 kW at 400°C but, during startup, the pipe must pass through temperature regions where heat-transfer rates are very low, e.g., 15 W at 120°C.

### Test 2

Another test of this pipe was made under similar conditions except that the heat-rejection rate was lowered by reducing the coupling of the heat sink with air in the calorimeter gap. In this case, a suc-

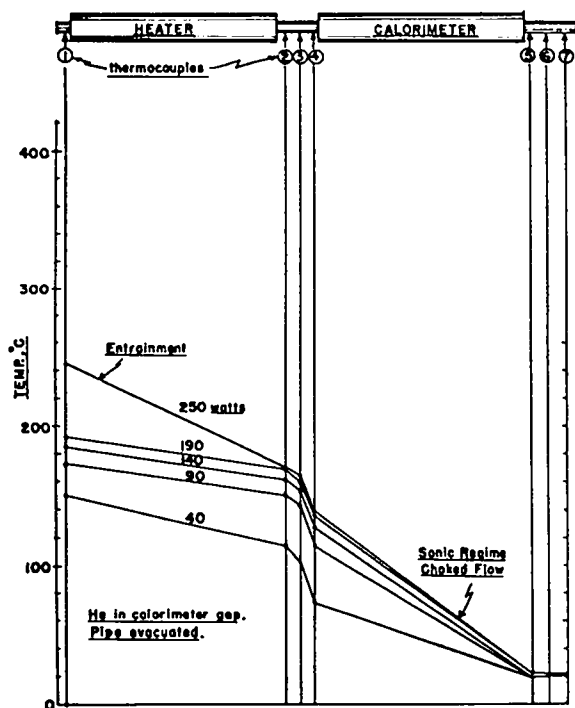


Fig. 4. Startup failure due to entrainment.

cessful startup was achieved even though the pipe operation passed through the sonic regime with choked flow and a limited heat-transfer rate. The heat-rejection rate was low enough for the condenser end to gradually heat up with a corresponding increase in vapor density and a reduction of vapor velocity at the evaporator exit. This enabled the pipe to move through the sonic-limit regime and come up to temperature as shown in Fig. 5. No operating limit was reached, and almost complete temperature recovery was obtained at the condenser end. The pipe could have been operated at much higher heat-transfer rates once it was up to temperature by gradually increasing the heat input and increasing the heat-sink coupling by substituting helium in the calorimeter gap.

### Test 3

The effect of a noncondensable gas on the startup dynamics of a heat pipe was demonstrated in this test. Instead of being completely evacuated, the pipe contained a small amount of noncondensable gas. The

presence of the gas effectively reduces the heat-rejection area and lowers the vapor velocity. The axial temperature drop along the evaporator is reduced, resulting in a higher vapor density at the evaporator exit and vapor velocities well below sonic. This produced a startup in the form of a wave front moving along the pipe as the heat input is increased (see Fig. 6). As the pipe temperature gradually increased, the gas was compressed more toward the end of the pipe and, at 1060 W, the pipe operation was essentially isothermal except for a small section at the end of the pipe due to the gas pocket. There was also a slight temperature recovery at Thermocouple 6, which is different from the type of pressure recovery in a converging-diverging nozzle. This type of recovery is a stagnation condition where kinetic energy is converted into heat because the heat pipe is a closed-end system while the nozzle is an open-ended system. With the noncondensable gas in the pipe, a successful startup was achieved even though the heat sink was closely coupled with a high heat-re-

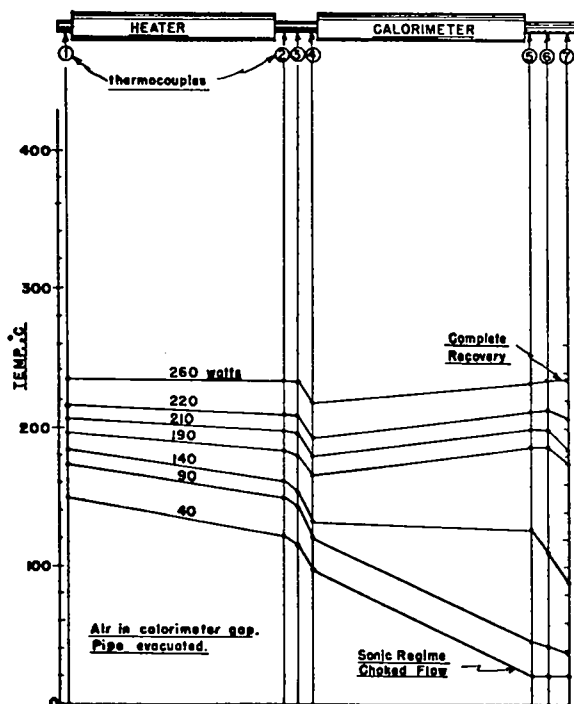


Fig. 5. Successful startup with reduced heat-sink coupling.

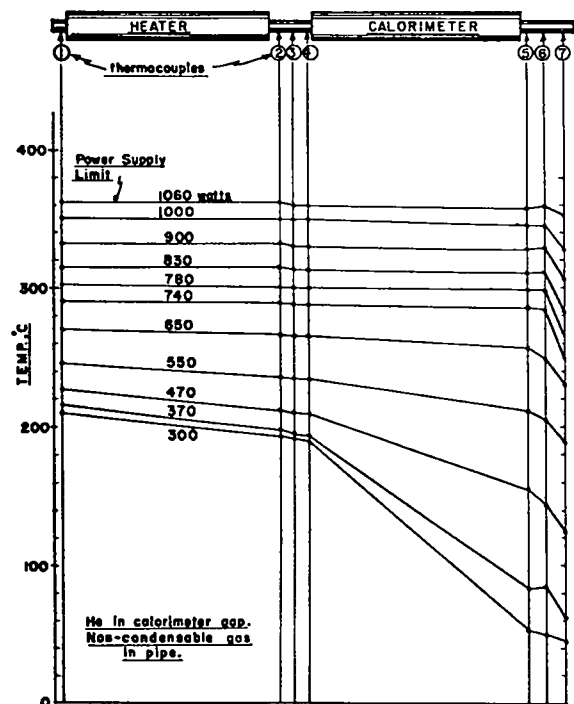


Fig. 6. Startup with noncondensable gas in pipe.

jection rate. No heat-pipe limitations were encountered and operation was essentially isothermal up to the limit of the power supply.

#### Test 4

In this test, a transient-state startup was made to observe the temperature recovery in a heat pipe with supersonic vapor velocities during startup from room temperature with a constant heat input of 300 W to the evaporator. The temperature gradients, as a function of time, are shown in Fig. 7. Although the vapor velocity was supersonic and choked vapor flow existed at the beginning of startup, the pipe passed through this regime and reached an isothermal operating level. This occurred because the heat-rejection rate was very low and, even with choked flow, there was sufficient continuum vapor flow to start temperature recovery at a relatively low temperature. Under these conditions the pipe was able to rise in temperature, with an increase in vapor density and a subsequent decrease in vapor velocity, before entrainment could cause failure. Although the heat input was higher than that which caused failure in

Test 1, a successful startup was achieved because the heat-rejection rate was very low.

#### STARTUP OF WATER HEAT PIPES

There is seldom any difficulty in starting up water heat pipes because of the relatively high vapor pressure of water at normal ambient temperatures. The high vapor density, associated with the high vapor pressure, and the high latent heat of vaporization of water result in a sonic-limit heat-transfer rate of 1 kW at 20°C. Because the design heat-transfer rate for many water heat pipes is only a fraction of this limit, the vapor velocities during startup are quite low and startup failures due to entrainment are not normally encountered. Another advantage of water as a working fluid is that at normal temperatures it is a liquid and does not require melting before fluid return to the evaporator can occur. Under certain conditions, however, it is possible to start up a water heat pipe from subzero temperatures with all the fluid in the frozen state. Starting up under these conditions may not seem typical of normal conditions, but it is of interest because most of the higher-temperature heat pipes have working fluids that remain solid well above ambient temperatures. Startup of these high-temperature pipes is similar to the startup of a water pipe from subzero temperatures. A startup from the frozen state is a function primarily of the heat-rejection rate at the condenser. The rejection rate must be low enough to enable the heat which is transferred to melt the fluid in the condenser and allow liquid return through the wick structure before the evaporator is depleted of fluid. A small amount of noncondensable gas in the pipe also aids in the startup by retarding the vapor flow so that the melting of the solid is done progressively along the pipe. This type of startup was demonstrated by a test in which a water heat pipe was cooled to -65°C in a vacuum chamber. With the pipe

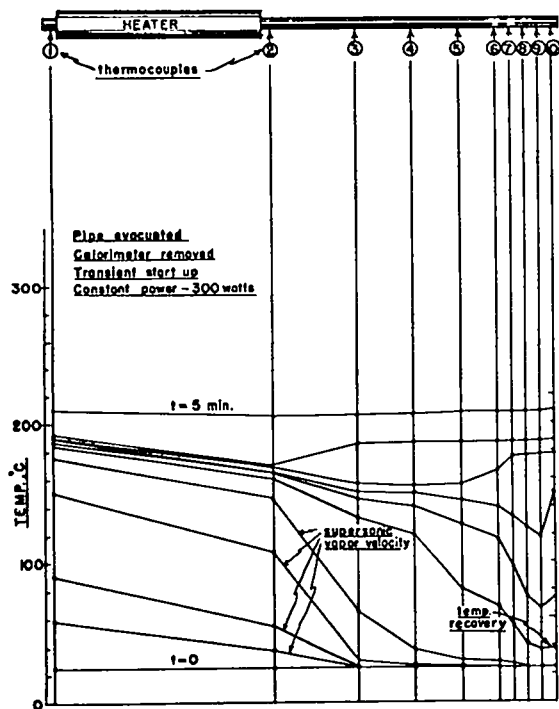


Fig. 7. Transient-state startup.

at  $-65^{\circ}\text{C}$ , 10 W were applied to the heater and temperatures were recorded at various time intervals as shown in Fig. 8. Even when all the water was frozen, heat was transferred along the pipe by sublimation. However, because the wick contained ice, there was no fluid return to the evaporator to replace the sublimed fluid. This was apparent from the rapid rise in heater temperature until Stations 1, 2, and 3 rose above the ice melting point. Water was then wicked into the heater area, and the temperature rise was arrested. This water was rapidly evaporated, and the vapor formed flowed to the end of the condenser where it again became ice. As a considerable portion of the total fluid was still ice, there was insufficient liquid flow into the heater area to prevent it from drying out and the temperature of this section again rose rapidly to  $104^{\circ}\text{C}$ . When the full length of the pipe was above the melting point, water could again wick into the heater area and the temperature of the heater dropped suddenly to  $44^{\circ}\text{C}$ . The pipe

then started to operate normally and gradually became isothermal. The startup was in the form of a temperature wave front moving along the pipe creating a transient temperature gradient. This was due to a small amount of noncondensable gas in the pipe which retarded the vapor flow and produced a variable heat-rejection area allowing the pipe to come up to temperature gradually. The gas was pushed toward the end of the pipe as the temperature increased and, at equilibrium temperature, was compressed into a very small volume so that no temperature gradient was apparent. A successful startup was achieved under these conditions because heat rejection was by radiation and extremely low, and the radiation area was automatically controlled by the presence of the noncondensable gas.

#### STARTUP OF ALKALI-METAL HEAT PIPES

The startup of heat pipes using alkali metals with melting points well above ambient temperatures is very similar to the subzero startup of water pipes. With the fluid in the solid state, startups are possible but are very dependent upon the heat-rejection rate. Many successful startups of these pipes have been made when heat rejection was by radiation; however, a series of tests made with a potassium pipe with a closely coupled heat sink showed that startups were difficult or impossible, depending upon the degree of coupling. The tests were made with a pipe having an annular-type wick structure and a water-cooled, gas-gap calorimeter for the heat-rejection system. The calorimeter gap was fitted with a helium supply tube, similar to that used in the mercury tests, so that the heat-sink coupling could be changed by a factor of four with air or helium in the gap. Tests made under different conditions indicated that, with high heat-rejection rates and a closely coupled heat sink, it was not possible to start the pipe. Three types of startup failures were encountered:

1. Depletion of evaporator fluid by

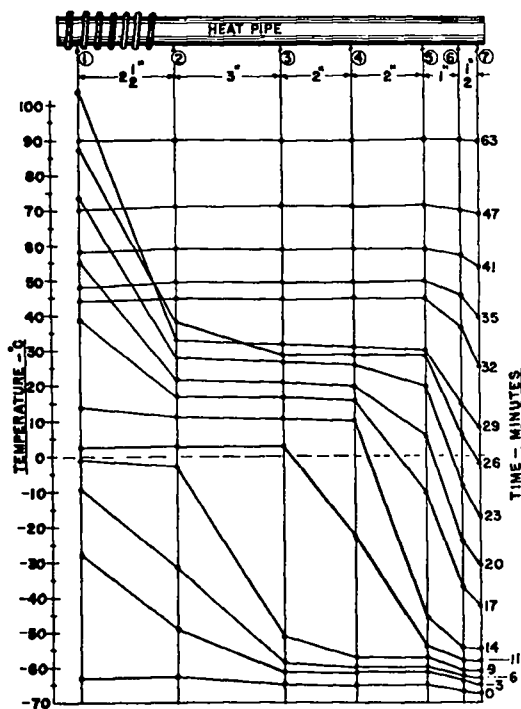


Fig. 8. Subzero startup of water heat pipe.

entrainment due to high vapor velocities.

2. Freezing of the condensed vapor preventing fluid return to the evaporator.
3. The pressure drop between the evaporator and condenser exceeding the capillary pumping force.

The first type of failure was the same as that encountered in the mercury heat-pipe startup tests. The high vapor velocities swept the liquid out of the wick structure and caused drying out and overheating of the evaporator section. The startup was made slowly with a low heat-rejection rate until all the fluid in the pipe was in the liquid state. Helium was then injected into the calorimeter gap to produce a high heat-rejection rate which resulted in high vapor velocities as the startup proceeded. Eventually, the high velocities resulted in sufficient interaction between the liquid and vapor to cause failure. The pipe was sonic-limited with the higher heat-rejection rate, and the heat-transfer rate was too low to raise the temperature of the condenser sufficiently to decrease the velocity and prevent entrainment failure. When the failure occurred, impingement of liquid particles at the condenser end of the pipe was audible. This type of failure is directly related to high vapor velocities.

The second type of failure is associated with the sonic-limit heat-transfer rate and a high heat-rejection rate. In this case, the limited heat transfer was not sufficient to raise the condenser temperature above the freezing point of the fluid and the condensing vapor was frozen out in the wick structure. This condition prevented fluid return to the evaporator and eventually caused depletion of fluid in the evaporator section and heat-pipe failure.

The third type of failure encountered was due to an attempt to start up rapidly with a high heat-rejection rate at the con-

denser. It is also related to the sonic limit because the heat-transfer rate was not sufficient to raise the condenser temperature. If the temperature of the condenser cannot rise, the vapor pressure remains essentially zero in that section. A high heat input with a low heat-transfer rate along the pipe due to choked flow causes the evaporator vapor pressure to increase rapidly, and, eventually, the pressure drop along the pipe can exceed the capillary pumping force of the wick structure. When this happens no liquid can return to the evaporator. For example, with a wick pore size of  $20\mu$ , the total capillary pumping force available is 94 Torr. The vapor pressure of potassium at  $572^{\circ}\text{C}$  is also 94 Torr, so, if the evaporator is heated to this temperature and the condenser section is maintained at ambient temperature by a high heat-rejection rate, the capillary force will be overcome by the vapor pressure drop. This leaves no pumping force available for liquid return to the evaporator section, and a failure will occur.

#### DISCUSSION

These tests demonstrate that the startup and operating characteristics of a heat pipe are very dependent upon the external conditions imposed upon it. The startup of a heat pipe generally involves high vapor velocities; in many cases the velocity can be sonic or supersonic. This results in choked vapor flow and limited heat-transfer rates. The sonic limit in itself is not a heat-pipe failure, and pipes can be started up through the sonic regime with no detrimental effects. Under certain conditions, however, the sonic limitation can disrupt fluid circulation to the extent where catastrophic failure can occur and startup is impossible. Even though a pipe could perform properly at design conditions, it may not be possible to reach the design level unless some method is incorporated to prevent failure during startup.

There is usually no difficulty in starting up a pipe designed for applications where heat rejection is by radiation. Heat rejection by radiation is a self-compensating system and automatically controls the heat-rejection rate. At low temperatures, the heat rejection is extremely small; the condenser section is essentially insulated during startup and can come up to temperature even though the heat-transfer rate may be sonic limited. As the temperature of the pipe gradually rises, the heat-rejection rate increases rapidly because radiation varies as the fourth power of temperature and, when the operating temperature is reached, the required heat rejection rate for design conditions is attained. Radiation heat rejection can therefore be considered as a variable insulation system, and startup difficulties are not normally encountered under these conditions.

For other applications where the heat pipe is closely coupled with a large heat sink, such as thermoelectric devices, the startup can be difficult or impossible. In this case, the startup problem should be considered in the system design. It may be necessary to incorporate a thermal barrier at the heat sink similar to the gas-gap calorimeter, and, although this would require the pipe to operate at higher temperatures, it may be necessary to provide a successful startup.

One method to aid in the startup of heat pipes is the addition of a small amount of inert, noncondensable gas such as argon. The gas has an effect similar to that of radiation heat rejection because it controls the heat-rejection rate and allows the pipe to gradually come up to temperature. This method is quite feasible for pipes with homogeneous wick structures but may cause problems with composite wicks. If any of the gas gets trapped in the liquid return path, it can migrate to the evaporator section and reduce or possibly eliminate the capillary pumping force.

There is no single solution to startup problems. Each application of heat pipes should be evaluated with regard to the startup dynamics as well as operating performance. If a startup problem does exist this must be considered in the system design with the solution depending upon the sonic limitations, the degree of heat sink coupling, and the external conditions to which the pipe is exposed.

#### ACKNOWLEDGMENTS

The assistance of A. G. Vaughan and J. R. Markham, LASL Group N-5, in the fabrication, welding, and assembly of the heat pipes used in these experiments is gratefully acknowledged.

## APPENDIX A

### A ONE-DIMENSIONAL, COMPRESSIBLE-FLOW HEAT PIPE ANALYSIS

#### NOMENCLATURE

- A - cross-sectional area of vapor passage.
- $c_v$  - vapor specific heat at constant volume.
- $c_p$  - vapor specific heat at constant pressure.
- f - friction factor.
- h - specific enthalpy of vapor.
- $h_L$  - specific enthalpy of liquid.
- $h_g$  - specific enthalpy of saturated vapor.
- $h_f$  - specific enthalpy of saturated liquid.
- $h_{fg}$  - enthalpy of vaporization (latent heat).
- k - ratio of specific heats of vapor.
- M - Mach number of vapor.
- p - static pressure of vapor.
- Q - heat transfer rate.
- R - gas constant.
- T - absolute temperature of vapor.
- V - vapor velocity.
- $V_L$  - liquid velocity
- W - molecular weight.
- w - vapor mass flow rate.
- $w_L$  - liquid mass flow rate.
- z - axial coordinate.
- $\rho$  - vapor density.

#### Subscripts and Superscripts

- o - evaporator entrance, stagnation station.
- 1 - evaporator exit station.
- \*
- s - saturation temperature.

#### INTRODUCTION

To develop useful relationships for pressure, temperature, and density changes encountered in the fluid circulation of heat pipes, the following analysis was developed based upon a one-dimensional flow model. The results can also be obtained from a general fluid flow development;<sup>7</sup> however, this analysis derives the relationship from basic principles applied directly to heat-pipe dynamics in an attempt to clarify the significance of the resulting expressions as applied to heat-pipe performance.

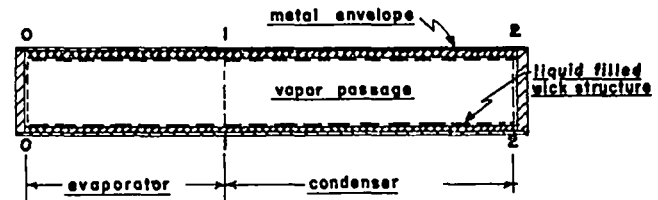


Fig. A-1. Schematic of heat pipe.

#### EVAPORATOR PRESSURE, TEMPERATURE, AND DENSITY RATIOS

A schematic representation of a heat pipe with control volumes for the evaporator and condenser regimes, indicated by dashed lines, is shown in Fig. A-1. The control surface is considered to be the vapor side of the vapor-liquid interface, and the cross-sectional area of the vapor passage is considered to be constant.

The evaporator pressure ratio  $p_o/p_1$  can be determined by a force-momentum balance in the evaporator control volume. For relatively high evaporation rates, inertial effects will dominate and frictional effects may be neglected. As indicated in Fig. A-2, the net force on the control volume in the z-direction is  $(p_o - p_1)A$ . The momentum transport in the z-direction at the upstream end of the evaporator (Section 0) is zero, and at the downstream end (Section 1) is  $(\rho_1 A V_1) V_1$ . The evaporated liquid crossing the circumferential portion of the control surface does so normal to the surface and, therefore, has no z-component of momentum. Setting the net force in the

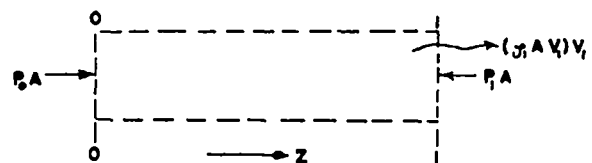


Fig. A-2. Evaporator control volume for force-momentum balance.

z-direction equal to the net efflux of momentum in the z-direction yields

$$(P_0 - P_1)A = (\rho_1 A V_1) V_1,$$

or

$$P_0 - P_1 = \rho_1 V_1^2. \quad (1)$$

If the vapor is assumed to obey the equation of state of a perfect gas,

$$P = \rho RT, \quad (2)$$

and

$$c_p - c_v = R. \quad (3)$$

The velocity of sound in a perfect gas is given by

$$V^* = \sqrt{kRT}. \quad (4)$$

The Mach number is defined as

$$M = V/V^*. \quad (5)$$

Using Eqs. (2), (4), and (5), Eq. (1) may be modified as follows:

$$\frac{P_0}{P_1} - 1 = \frac{\rho_1 V_1^2}{P_1} = \frac{M_1^2 k R T_1}{R T_1} = k M_1^2,$$

or

$$\frac{P_0}{P_1} = 1 + k M_1^2. \quad (6)$$

The maximum possible velocity which can be developed at the evaporator exit is the sonic velocity ( $M_1 = 1$ ). This is analogous to the maximum velocity which can be developed at the throat of a nozzle. Thus, the maximum evaporator pressure ratio, which corresponds to sonic flow at the exit, is

$$\frac{P_0}{P_1^*} = 1 + k. \quad (7)$$

If  $k$  is evaluated corresponding to the temperature at Section 1, Eqs. (6) and (7) are valid irrespective of any variation in  $k$  along the evaporator.

The evaporator temperature ratio  $T_0/T_1$  can be determined from an energy balance on the evaporator control volume. It is assumed that work done by shear forces on the control volume, heat transfer to the vapor in the control volume by conduction and radiation, and the kinetic energy carried

into the control volume by evaporated liquid may all be neglected compared to the enthalpy of the evaporated liquid. In addition it is assumed that the evaporated liquid enters the control volume at a uniform temperature equal to the temperature  $T_0$  at the upstream end of the evaporator. Assuming a constant specific heat  $c_p$ , the energy transport rate across the circumferential control surface due to evaporated liquid will then be  $w(c_p T_0)$ . The energy transport across Station 0 will be zero and across Station 1 will be  $w(c_p T_1 + V_1^2/2)$ , which is the enthalpy transport plus the kinetic energy transport. These energy flows are depicted in Fig. A-3.

For steady-state conditions, the energy balance is then

$$w(c_p T_0) = w(c_p T_1 + V_1^2/2),$$

which may be rearranged to give

$$\frac{T_0}{T_1} = 1 + \frac{V_1^2}{2 c_p T_1}. \quad (8)$$

Using Eqs. (3), (4), and (5) evaluated at Station 1, Eq. (8) may be modified as follows:

$$\frac{T_0}{T_1} = 1 + \frac{M_1^2 k R T_1}{2 c_p T_1} = 1 + \frac{M_1^2 k (c_p - c_v)}{2 c_p},$$

or

$$\frac{T_0}{T_1} = 1 + \frac{k-1}{2} M_1^2. \quad (9)$$

The maximum evaporator temperature ratio corresponding to sonic flow at the exit ( $M_1 = 1$ ) is

$$\frac{T_0}{T_1^*} = 1 + \frac{k-1}{2} = \frac{k+1}{2}. \quad (10)$$

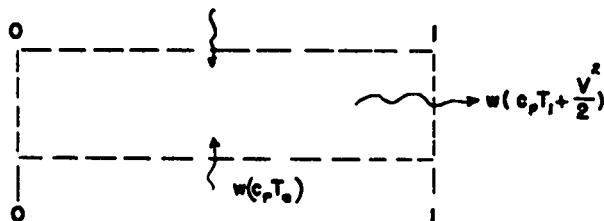


Fig. A-3. Evaporator control volume for energy balance.

With regard to the equation of state of vapor, Eqs. (9) and (10) depend, in the strict sense, only on the assumptions that  $c_p$  is constant and that the vapor obeys the perfect gas laws. However, the assumption of  $c_p$  constant for a perfect gas implies that  $c_v$ , and therefore  $k$ ,  $W$ , and  $R$  will all be constant.

The evaporator density ratio,  $\rho_o/\rho_1$ , can now be computed. From Eq. (2),

$$\frac{\rho_o}{\rho_1} = \frac{P_o}{P_1} \frac{T_1}{T_o}.$$

Substitution from Eqs. (6) and (9) results in

$$\frac{\rho_o}{\rho_1} = \frac{1 + k M_1^2}{(1 + \frac{k-1}{2} M_1^2)}, \quad (11)$$

for the density ratio. At sonic conditions ( $M_1 = 1$ ),

$$\frac{\rho_o}{\rho_1} = 2. \quad (12)$$

The density ratio for sonic conditions is independent of  $k$ .

It is of interest to note that the various property ratios that are applicable for the one-dimensional model of the vapor flow in a heat-pipe evaporator section are summarized in Table 8.3, p. 239 of Vol. I of the well-known work on compressible flow by A. H. Shapiro.<sup>4</sup> The appropriate column to utilize is the one headed "Gas injection only,  $y = 0$ ,  $dA = 0$ ,  $dT_o = 0$ ,  $f = 0$ ." This heading implies the following conditions and assumptions:

- i)  $y = 0$ , gas injection normal to main flow stream, no axial velocity component.
- ii)  $dA = 0$ , constant flow cross-sectional area.
- iii)  $dT_o = 0$ , no change in stagnation temperature, and neglect of kinetic energy carried into main stream by the injected gas.
- iv)  $f = 0$ , neglect frictional effects.

These are identical to the assumptions utilized in the preceding derivation.

Of the three vapor properties, pressure, temperature, and density, only the pressure will be very nearly uniform across the cross section in a heat pipe. The quantities  $T_1$  and  $\rho_1$  as determined from Eqs. (9) and (11) must be regarded as approximations to the average vapor temperature and density existing at the evaporator exit of a heat pipe.

Direct measurements of the vapor properties in an operating heat pipe are difficult. However, with a short insulated section just upstream of the evaporator and another insulated section between evaporator and condenser, thermocouples attached to the pipe wall at these sections will indicate temperature closely approximating the local liquid-vapor interface saturation temperature  $T_{os}$  and  $T_{1s}$ . Because stagnation conditions exist at the upstream end of the evaporator, properties are uniform across the cross section and  $T_o = T_{os}$ . However, the temperature distribution across Section 1 is not uniform. Hence,  $T_1 \neq T_{1s}$ . One may proceed by taking  $P_o$  and  $P_1$  to be saturation pressures evaluated at  $T_{os}$  and  $T_{1s}$ . The Mach number,  $M_1$ , and estimates of the average vapor temperature and density at the evaporator exit may then be calculated from Eqs. (6), (9), and (11), respectively. In calculating  $\rho_1$ , from Eq. (11),  $\rho_o$  is taken as the saturation density corresponding to  $T_o$ . For sonic flow at the evaporator exit, Eqs. (7), (10), and (12) apply.

#### Calculation of the Heat Rate Including the Sonic Limit

The heat rate to the evaporator section of the heat pipe can be evaluated in terms of flow conditions at evaporator Station 1 by an energy balance on a control volume enclosing the entire evaporator section including the metal envelope, the liquid-filled wick structure, and the vapor region (see Fig. A-4). In the heat-pipe regime as

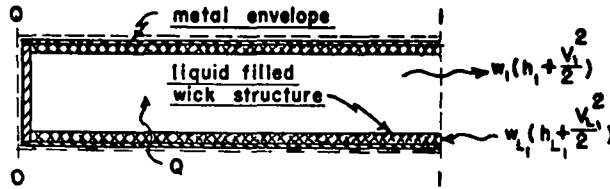


Fig. A-4. Evaporator control volume for heat-transfer-rate calculations.

defined by Cotter,<sup>1</sup> axial temperature gradients will be relatively small so that axial conduction in vapor, liquid-filled wick structure, and metal envelope are neglected. Thus, for steady-state conditions the energy balance illustrated in Fig. A-4 is given by

$$Q = w_1 \left( h_1 + \frac{V_1^2}{2} \right) - w_{L1} \left( h_{L1} + \frac{V_{L1}^2}{2} \right),$$

or, since by conservation of mass for the control volume of Fig. A-4,  $w_1 = w_{L1}$ , and  $w_1 = \rho_1 A V_1$ ,

$$Q = \rho_1 A V_1 \left[ \left( h_1 - h_{L1} \right) + \frac{V_1^2}{2} - \frac{V_{L1}^2}{2} \right].$$

The difference in kinetic energy between vapor and liquid will be negligible compared to the enthalpy difference. Furthermore, consistent with the one-dimensional model for the vapor flow, the specific enthalpy of the vapor will be equal to the saturation enthalpy because the vapor is in equilibrium with the liquid at the vapor-liquid interface. Due to the radial heat conduction through the liquid, it will be superheated at points away from the vapor-liquid interface. However, this superheat will almost always be small enough so that no significant error is introduced if the specific enthalpy of the liquid is also assumed to be the saturation value. Thus, we have for the heat rate in terms of conditions at the evaporator exit,

$$Q = \rho_1 A V_1 (h_{g1} - h_{f1}) = (\rho_1 A V_1) h_{fg1}. \quad (13)$$

A useful relation, particularly for the heat-pipe experimentalist, can be

obtained for the heat rate as a function of the evaporator pressure ratio. Introducing the Mach number into the basic heat rate Eq. (13) results in

$$Q = \rho_1 A M_1 \sqrt{kRT_1} h_{fg}$$

From this point on, the Subscript 1 will be omitted from the enthalpy of vaporization,  $h_{fg}$ , since it is not a strong function of temperature. However, it should be kept in mind that it is best to evaluate it corresponding to the saturation temperature at Station 1.

If  $T_1$  and  $\rho_1$  are replaced utilizing Eqs. (9) and (11), respectively, one obtains

$$Q = M_1 \frac{\sqrt{1 + \frac{k-1}{2} M_1^2}}{1 + k M_1^2} \rho_o A \sqrt{kRT_o} h_{fg}. \quad (14)$$

Solving Eq. (6) for  $M_1$  and substituting in (14) gives

$$Q = \frac{1}{(P_o/P_1)} \sqrt{\frac{1}{k} \left( \frac{P_o}{P_1} - 1 \right) \left[ 1 + \frac{k-1}{2k} \left( \frac{P_o}{P_1} - 1 \right) \right]} \rho_o A \sqrt{kRT_o} h_{fg}, \quad (15)$$

for the heat rate in terms of the stagnation conditions at the upstream end of the evaporator and the evaporator pressure ratio.

The heat rate corresponding to sonic conditions at the evaporator exit can now be obtained from Eq. (14) by setting  $M_1 = 1$ , or from Eq. (15) by setting  $P_o/P_1 = 1 + k$ . In either case, the result is

$$Q^* = \frac{\rho_o A \sqrt{kRT_o} h_{fg}}{\sqrt{2(k+1)}}, \quad (16)$$

for sonic limiting heat rate in terms of stagnation conditions at the upstream end of the evaporator. Reasonably good measurements of  $T_o$  are not too difficult to obtain;  $\rho_o$  is then taken as the saturation density corresponding to  $T_o$ .

The square-root term in the numerator on the right-hand side of Eq. (16) is the velocity of sound corresponding to conditions at the upstream end of the evaporator and may be represented as  $V_o^*$ . Thus, Eq. (16) is often written in the form

$$\frac{Q^*}{A} = \frac{\rho_o V_o^* h_{fg}}{\sqrt{2(k+1)}} \quad (17)$$

This equation was first introduced by Levy.<sup>3</sup> However, his derivation required the assumption of uniform mass injection (of evaporated liquid) plus the requirement that

$$\frac{2(h-h_g) + V^2 - V_n^2}{2 c_p T} \ll M^2 (k-1) + 2, \quad (18)$$

where  $h$  is the enthalpy of the main vapor stream,  $h_g$  is the enthalpy of the evaporated liquid (saturated), and  $V_n$  is the normal velocity of the evaporated liquid entering the vapor stream. The derivation outlined here shows that the equation is valid also for the assumption that the evaporated liquid enters the vapor stream at  $T_o$ , without the explicit requirements of uniform mass injection and the inequality expressed in Eq. (18). Either set of assumptions will be reasonable for most heat-pipe situations. The assumption used here has the advantage that it results in a simpler, more straightforward derivation. Experimental verification of Eq. (16) has been provided by Kemme.<sup>2</sup>

Convenient dimensionless forms for Eqs. (14) and (15) can be obtained by dividing them by Eq. (16). In this way one obtains

$$\frac{Q}{Q^*} = \frac{M_1 \sqrt{2(k+1)} \left(1 + \frac{k-1}{2} M_1^2\right)}{1 + k M_1^2} \quad (19)$$

for the heat rate as a fraction of the sonic limiting heat rate in terms of the Mach number at the evaporator exit, and

for the heat-rate fraction as a function of the evaporator pressure ratio.

Again, it is of interest to note that Eqs. (19) and (20) can be obtained fairly directly utilizing Table 8.3 in Shapiro.<sup>7</sup> First, the heat rate for a specified condition at the evaporator exit may be written as  $Q = w_1 h_{fg}$ . For sonic conditions  $Q^* = w_1^* h_{fg}$ . Thus,  $Q/Q^* = w_1/w_1^*$ . Table 8.3 gives the ratio  $w_1/w_1^*$  directly as a function of Mach number. For the case of "gas injection only,  $y = 0$ ," this function is identical to the right-hand side of Eq. (19) and Eq. (20) may then be obtained by substituting for  $M_1$  in terms of  $P_o/P_1$  utilizing Eq. (6) or its equivalent obtained utilizing Table 8.3 of Ref. 7.

Equations (19) and (20) are plotted in Figs. A-5 and A-6 for both monatomic vapors ( $k = 5/3$ ) and diatomic vapors ( $k = 7/5$ ). It can be observed that  $Q/Q^*$  is not strongly dependent on  $k$  over this range. For Mach numbers less than about 0.3, compressibility effects may be reasonably neglected. Figure A-5 shows that this will correspond to heat rates up to about 60% of the sonic limiting heat rate.

Figure A-6 is useful for comparison with experimental results. Kemme<sup>2</sup> obtained good agreement with Eq. (19) for sodium and cesium heat pipes. Note that the heat rate is relatively independent of the pressure ratio as the sonic limit is approached. For instance, at a pressure ratio of 1.6, which is 60% of the maximum pressure ratio for a monatomic vapor, the heat rate already exceeds 90% of the sonic limiting heat rate.

---


$$\frac{Q}{Q^*} = \frac{1}{(P_o/P_1)} \sqrt{2 \left(\frac{P_o}{P_1} - 1\right) \frac{k+1}{k} \left[1 + \frac{k-1}{k} \left(\frac{P_o}{P_1} - 1\right)\right]} \quad (20)$$


---

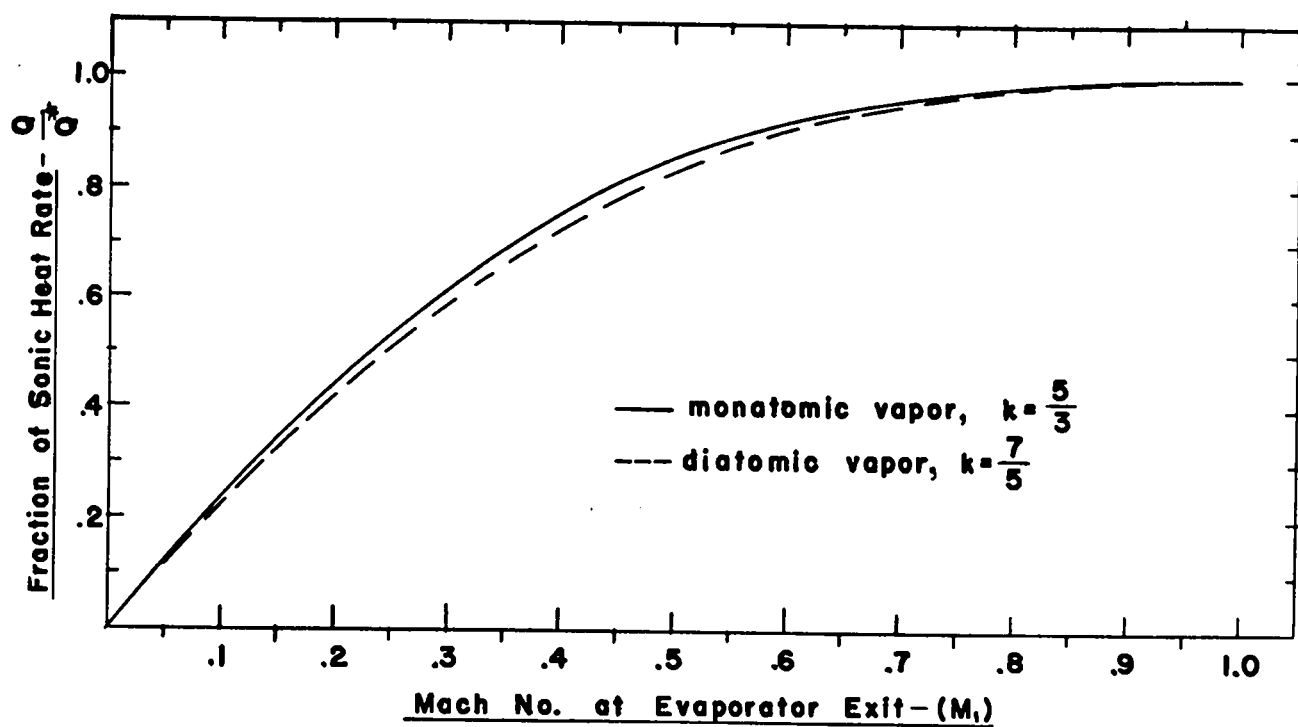


Fig. A-5. Fraction of sonic heat-transfer rate vs Mach number.

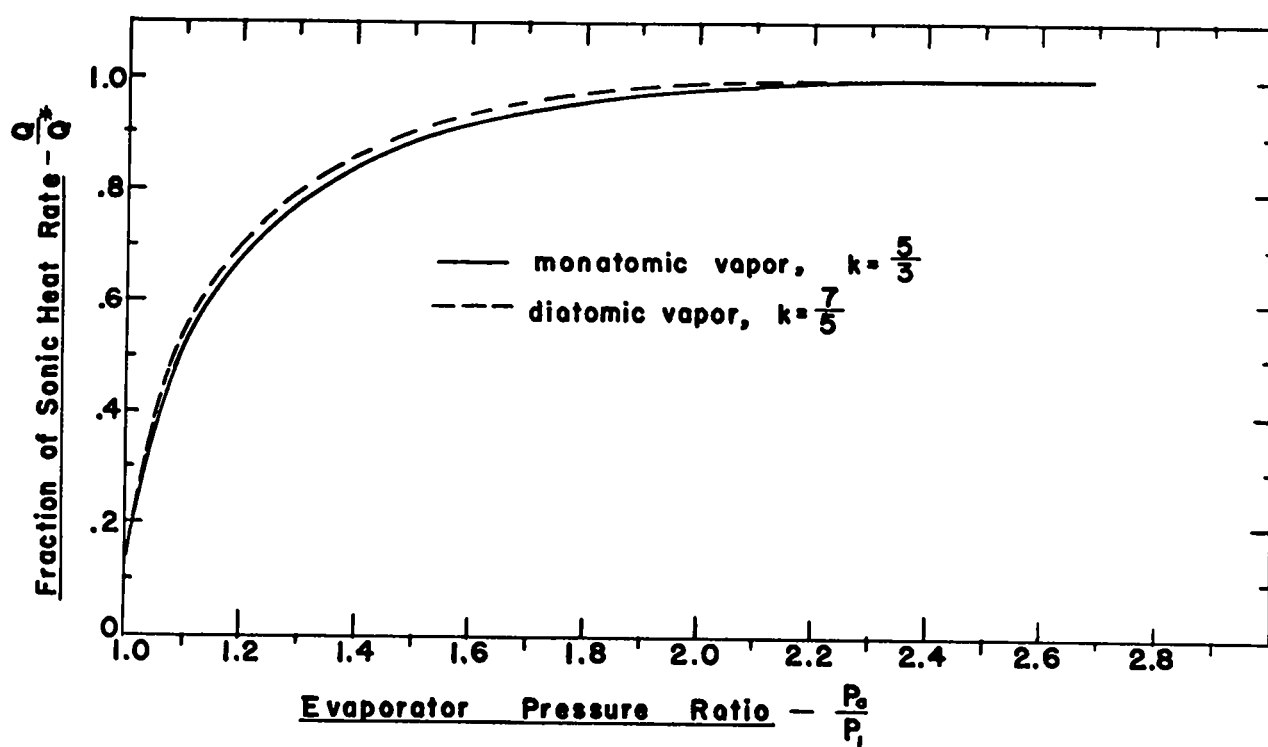


Fig. A-6. Fraction of sonic heat-transfer rate vs pressure ratio.

APPENDIX B  
SONIC LIMIT TABLES FOR

Water

Mercury

Cesium

Potassium

Sodium

Lithium

TABLE I. SONIC LIMIT FOR WATER

$T_o$ Evaporator Entrance, °C	$P_o$ Vapor Pressure, Torr	$P_o \times 10^5$ Vapor Density, g/cm <sup>3</sup>	$L$ Heat of Vaporization, W-sec/g	$\delta$ Surface Tension, dyne/cm	$V_s$ Sonic Velocity, cm/sec	$T_{w1}$ Evaporator Exit, °C	Axial $\Delta T$ Along Evaporator Wall, °C	Maximum Axial Heat Transfer at Sonic Velocity, W/cm <sup>2</sup>
0	4.57	.47	2488	76.4	40,780	-11	11	229
10	9.21	.94	2471	74.8	41,520	-2	12	449
20	17.54	1.73	2448	73.0	42,250	7	13	1,034
30	31.80	3.03	2426	71.2	42,960	16	14	1,439
40	55.32	5.11	2404	69.6	43,660	25	15	2,494
50	92.5	8.32	2379	67.8	44,360	34	16	4,083
60	149.4	13.1	2356	66.0	45,040	43	17	6,415
70	233.7	19.8	2331	64.2	45,710	52	18	9,810
80	355.1	29.4	2307	62.4	46,370	60	20	14,630
90	525.8	42.4	2281	60.3	47,020	69	21	21,152
100	760.0	59.8	2255	58.7	47,670	78	22	29,900
110	1,074.6	82.7	2228	56.9	48,300	87	23	41,390
120	1,489.0	112.0	2200	55.0	48,930	95	25	55,080
130	2,026.0	150.0	2171	53.1	49,550	104	26	75,040
140	2,711.0	197.0	2141	51.2	50,160	113	27	98,390
150	3,571.0	255.0	2110	49.2	50,760	121	29	127,030
160	4,636.0	327.0	2078	47.2	51,360	130	30	162,310
170	5,941.0	413.0	2046	45.3	51,950	138	32	204,150
180	7,520.0	515.0	2012	43.3	52,530	146	34	253,160
190	9,413.0	639.0	1977	41.0	53,110	155	35	312,900
200	11,659.0	784.0	1941	39.0	53,680	163	37	379,900

TABLE II. SONIC LIMIT FOR MERCURY

$T_o$ Evaporator Entrance, °C	$P_o$ Vapor Pressure, Torr	$\rho_o \times 10^5$ Vapor Density, g/cm <sup>3</sup>	$L$ Heat of Vaporization, W-sec/g	$\delta$ Surface Tension, dyne/cm	$V_s$ Sonic Velocity, cm/sec	$T_{w1}$ Evaporator Exit, °C	Axial $\Delta T$ Along Evaporator Wall, °C	Maximum Axial Heat Transfer at Sonic Velocity, W/cm <sup>2</sup>
120	.75	.7	303.3	452	16,450	100	20	15
140	1.85	1.5	302.6	447	16,870	118	22	33
160	4.20	2.9	302.0	442	17,270	136	24	65
180	8.80	6.5	301.3	437	17,670	153	27	150
200	17.3	11.7	300.6	432	18,010	171	29	274
220	32.1	21.0	300.0	427	18,430	188	32	503
240	56.8	36.0	299.4	422	18,800	206	34	877
260	96.3	60.0	298.7	417	19,160	223	37	1,490
280	156.9	95.0	298.1	412	19,520	241	39	2,390
300	246.8	143.0	297.5	407	19,870	258	42	3,660
320	376.3	212.0	296.8	402	20,210	276	44	5,510
340	557.9	298.0	296.2	397	20,550	293	47	7,850
360	806.2	412.0	295.7	393	20,800	310	50	11,010
380	1,138.4	562.0	294.8	388	21,210	327	53	15,210
400	1,574.1	758.0	294.1	383	21,530	344	56	20,780
420	2,210.0	980.0	293.6	378	21,850	361	59	27,220
440	2,941.0	1,250.0	293.3	373	22,160	378	62	35,170
460	3,836.0	1,587.0	292.7	368	22,470	394	66	45,180
480	4,993.0	2,040.0	291.9	363	22,780	410	70	58,710
500	6,361.0	2,500.0	291.3	358	23,080	426	74	72,750
520	8,010.0	3,100.0	290.5	353	23,370	442	78	91,120
540	10,184.0	3,800.0	289.5	348	23,670	458	82	112,700
560	12,196.0	4,550.0	288.9	343	23,960	474	86	136,310
580	14,896.0	5,400.0	288.1	339	24,240	490	90	163,260
600	17,974.0	6,330.0	287.6	334	24,520	506	94	193,240

TABLE III. SONIC LIMIT FOR CESIUM								
$T_0$ Evaporator Entrance, °C	$P_0$ Vapor Pressure, Torr	$\rho_0 \times 10^5$ Vapor Density, g/cm <sup>3</sup>	L Heat of Vaporization, W-sec/g	$\delta$ Surface Tension, dyne/cm	$V_s$ Sonic Velocity, cm/sec	$T_{w1}$ Evaporator Exit, °C	Axial $\Delta T$ Along Evaporator Wall, °C	Maximum Axial Heat Transfer at Sonic Velocity, W/cm <sup>2</sup>
300	1.78	.60	545.0	61.5	24,410	264	36	35
320	2.80	.96	542.5	60.5	24,840	283	37	56
340	4.23	1.52	539.5	59.5	25,250	301	39	90
360	7.0	2.37	537.0	58.3	25,660	318	42	141
380	10.8	3.65	534.0	57.3	26,070	336	44	220
400	16.2	5.40	531.5	56.2	26,460	353	47	329
420	24.2	7.90	528.5	55.1	26,850	370	50	485
440	34.0	11.3	526.0	54.0	27,240	387	53	701
460	47.0	15.7	523.0	53.0	27,620	403	57	982
480	62.5	21.2	520.5	51.8	27,990	420	60	1,457
500	83.0	27.5	518.0	50.7	28,360	436	64	1,749
520	107.0	35.5	515.0	49.7	28,720	453	67	2,270
540	138.0	45.0	512.5	48.6	29,080	469	71	2,900
560	178.0	56.0	509.6	47.5	29,440	485	75	3,637
580	223.0	69.0	507.0	46.5	29,790	501	79	4,510
600	280.0	83.0	504.0	45.5	30,140	518	82	5,460

TABLE IV. SONIC LIMIT FOR POTASSIUM

$T_o$ Evaporator Entrance, °C	$P_o$ Vapor Pressure, Torr	$\rho_o \times 10^5$ Vapor Density, g/cm <sup>3</sup>	$L$ Heat of Vaporization, W-sec/g	$\delta$ Surface Tension, dyne/cm	$V_s$ Sonic Velocity, cm/sec	$T_{w1}$ Evaporator Exit, °C	Axial $\Delta T$ Along Evaporator Wall, °C	Maximum Axial Heat Transfer at Sonic Velocity, W/cm <sup>2</sup>
360	1.57	.20	2129	97.6	47,300	323	37	87
380	2.50	.29	2120	96.3	48,040	341	39	128
400	4.00	.42	2114	95.0	48,770	359	41	186
420	6.20	.62	2106	93.7	49,490	377	43	277
440	9.50	.92	2097	92.5	50,200	394	46	419
460	14.0	1.32	2089	91.2	50,900	412	48	608
480	20.3	1.87	2080	89.8	51,590	430	50	869
500	29.0	2.62	2072	88.5	52,270	447	53	1,230
520	40.0	3.65	2062	87.2	52,940	464	56	1,725
540	55.0	4.85	2053	86.0	53,600	481	59	2,310
560	75.0	6.15	2044	84.7	54,260	499	61	2,950
580	102.0	8.10	2034	83.3	54,190	516	64	3,920
600	132.0	10.2	2024	82.0	55,550	533	67	4,965
620	170.0	12.8	2013	80.7	56,180	550	70	6,266
640	215.0	16.0	2003	79.4	56,810	565	75	7,880
660	272.0	20.0	1992	78.1	57,420	580	80	9,900

TABLE V. SONIC LIMIT FOR SODIUM								
$T_o$ Evaporator Entrance, °C	$P_o$ Vapor Pressure, Torr	$\rho_o \times 10^5$ Vapor Density, g/cm <sup>3</sup>	$L$ Heat of Vaporization, W-sec/g	$\delta$ Surface Tension, dyne/cm	$V_s$ Sonic Velocity, cm/sec	$T_{w1}$ Evaporator Exit, °C	Axial $\Delta T$ Along Evaporator Wall, °C	Maximum Axial Heat Transfer at Sonic Velocity, W/cm <sup>2</sup>
440	1.00	.053	4320	157	65,550	404	36	65
460	1.80	.082	4297	155	66,410	421	39	101
480	2.85	.125	4277	153	67,310	439	41	156
500	4.30	.190	4255	151	68,200	456	44	239
520	6.20	.285	4233	149	69,080	474	46	361
540	8.70	.410	4213	147	69,940	491	49	523
560	12.3	.570	4193	145	70,800	509	51	732
580	17.0	.790	4172	143	71,640	526	54	1,022
600	23.5	1.06	4152	141	72,480	544	56	1,380
620	31.5	1.43	4132	139	73 300	561	59	1,875
640	43.0	1.90	4112	137	74,120	579	61	2,509
660	59.0	2.50	4092	135	74,930	596	64	3,318
680	79.0	3.30	4071	133	75,730	613	67	4,404
700	104.0	4.25	4052	131	76,520	631	69	5,704
720	137.0	5.40	4032	129	77,300	648	72	7,286
740	178.0	6.90	4012	127	78,070	666	74	9,356
760	225.0	8.50	3993	125	78,840	683	77	11,580
780	282.0	10.3	3975	123	79,600	700	80	14,110
800	345.0	12.7	3955	121	80,350	718	82	17,470

TABLE VI. SONIC LIMIT FOR LITHIUM

$T_o$ Evaporator Entrance, °C	$P_o$ Vapor Pressure, Torr	$\rho_o \times 10^5$ Vapor Density, g/cm <sup>3</sup>	$L$ Heat of Vaporization, W-sec/g	$\delta$ Surface Tension, dyne/cm	$v_s$ Sonic Velocity cm/sec	$T_{w1}$ Evaporator Exit, °C	Axial $\Delta T$ Along Evaporator Wall, °C	Maximum Axial Heat Transfer at Sonic Velocity, W/cm <sup>2</sup>
800	2.75	.07	21,310	323	146,110	748	52	943
820	3.75	.08	21,240	320	147,450	765	55	1,110
840	5.1	.10	21,160	317	148,790	782	58	1,390
860	6.7	.12	21,130	314	150,120	800	60	1,675
880	8.9	.15	21,050	311	151,440	817	63	2,070
900	11.4	.18	20,940	308	152,750	834	66	2,492
920	14.8	.22	20,900	305	154,050	852	68	3,219
940	19.0	.26	20,790	302	155,330	869	71	3,635
960	24.5	.31	20,720	299	156,610	886	74	4,355
980	31.0	.37	20,640	297	157,870	903	77	5,219
1000	39.0	.43	20,574	294	159,130	920	80	6,090
1020	49.0	.51	20,500	291	160,370	938	82	7,260
1040	62.0	.62	20,430	288	161,610	954	85	8,860
1060	77.0	.73	20,350	285	162,840	972	88	10,470
1080	95.0	.87	20,280	282	164,050	989	91	12,530
1100	118.0	1.02	20,200	279	165,260	1,007	93	14,740
1120	143.0	1.20	20,130	276	166,460	1,024	96	17,410
1140	173.0	1.42	20,060	273	167,650	1,041	99	20,670
1160	210.0	1.66	19,990	270	168,830	1,058	102	24,250
1180	250.0	1.95	19,900	267	170,010	1,076	104	28,560
1200	295.0	2.27	19,840	265	171,170	1,093	107	33,370

#### REFERENCES

1. T. P. Cotter, "Theory of Heat Pipes," Los Alamos Scientific Laboratory Report LA-3246-MS (1965).
2. J. E. Kemme, "Ultimate Heat Pipe Performance," IEEE Trans. Electron Devices, Vol. ED-16, No. 8, Aug. 1969.
3. E. K. Levy, "Theoretical Investigation of Heat Pipes," Aviation and Space Conference, Beverly Hills, Calif., 1968.
4. T. P. Cotter, "Heat Pipe Startup Dynamics," IEEE Thermionic Conversion Specialist Conference, Palo Alto, Calif., 1967.
5. J. E. Deverall, "Mercury as a Heat Pipe Fluid," Los Alamos Scientific Laboratory Report LA-4300-MS (1970).
6. J. E. Kemme, "High Performance Heat Pipes," IEEE Thermionic Conversion Specialist Conference, Palo Alto, Calif., 1967.
7. A. H. Shapiro, The Dynamics and Thermodynamics of Compressible Flow, Vol. I, The Ronald Press Co., New York, 1953.

#### BIBLIOGRAPHY

1. Handbook of Physics and Chemistry, Chemical Rubber Publishing Co.
2. Liquid-Metals Handbook, Atomic Energy Commission, Department of the Navy, 1952.
3. R. T. Caldwell and D. M. Walley, "Physical and Thermodynamic Properties of Potassium," Air Force Aero Propulsion Laboratory, technical report AFAPL-TR-66-104 (1966).
4. W. D. Weatherford, Jr., J. C. Tyler, and P. M. Ku, "Properties of Inorganic Energy-Conversion and Heat Transfer Fluids for Space Applications," Southwest Research Institute, 1961.
5. W. Frank, J. T. Smith, and K. M. Taylor, "Heat Pipe Design Manual," (1967), Martin Nuclear, Martin-Marietta.